Title: Spray coating vs. immersion for self-assembly of gemini perfluorinated phosphonic acids on indium tin oxide

Authors: Gaëlle Anne Léonie Andreatta*, Nicolas Blondiaux, Julien Gay, Samuel Unterhofer, Agata Lachowicz, Antonin Faes

Affiliation: Centre Suisse d'électronique et de Microtechnique CSEM, 1 rue Jaquet-Droz, CH-2002 Neuchâtel, Switzerland

* Corresponding author

gaelle.andreatta@csem.ch

Abstract:

Self-assembled monolayers (SAMs) are widely used to engineer the surface properties of metals and metal oxide layers. This article reports the fabrication of gemini perfluorinated phosphonic acids SAMs on indium tin oxide (ITO). The self-assembled monolayers are to be used for patterning nickel lines by electroplating on ITO in order to obtain low-cost conductor grids on heterojunction solar cells. The aim is to develop large-scale, low-cost processes that will both reduce production times and produce strong, covalently bonded monolayers of phosphonic acids on metal oxide surfaces along with uniform coverage. The gemini perfluorinated phosphonic acid provides extremely high hydrophobicity at the surface of ITO with a static contact angle of water above 115 ° and a remarkably low hysteresis of approximately 15 ° between advancing and receding contact angles. Well-known octadecylphosphonic acid is used as a reference material. Two deposition methods, by immersion and by spray-coating, are compared for the self-assembly of the molecules. The effect of the solvents used during the immersion, spray-coating, and rinsing steps are investigated. The surface properties are characterized by atomic

force microscopy, contact angle measurements, and attenuated total reflectance Fourier-transform infrared spectroscopy.

Keywords:

Self-assembled monolayers; Phosphonic acids; Perfluorinated self-assembled monolayers; Indium tin oxide; Spray-coating

Highlights:

1. Uniform gemini perfluorinated phosphonic acid monolayers are demonstrated.
2. Two different methods, spray-coating and immersion were compared and characterized.
3. Effects of spray and immersion solvents on the self-assembly were investigated.
4. Multilayers and spinodal dewetting were shown to depend on solvent compatibility.

1. Introduction

Self-assembled monolayers (SAMs) have generated widespread research interest due to their applications related to wettability control, corrosion resistance, sensors, adhesion, lubrication, controlled surface patterning, and, in general, the modification of surface properties and interfacial design [1–3]. Alkane-thiolates or dialkyl disulfides on gold [4–6] and silane-based molecules on silicon oxide SAMs have been extensively studied in the last few decades [7–10]. Phosphate, phosphonic acid (PA), and phosphonate-based SAMs have been attracting increased attention as these chemical functionalities attach to several metals or metal oxides, thus expanding the types of substrates that may be modified and coated [11–16].

PA SAMs on indium tin oxide (ITO) are of particular interest due to the extensive use of this material in the electronics and photovoltaics industry. PA SAMs have been reported to act as a resist for wet etching [17], to protect surfaces against corrosion [2, 18], to modify the work function of transparent conductive oxides [19–22], and as a patterning layer for the metallization of heterojunction solar cells [23]. Recently, PA SAMs have also been shown to improve the perovskite solar cell efficiency when used as or within charge-transporting layers [24–27].

Currently, the dominant deposition protocol for PA SAMs on ITO is the immersion of a cleaned and activated substrate in a PA solution with immersion times lasting anywhere from a few minutes to a couple of hours or even days [14], [28]. The favored deposition method for perovskite solar cells applications are reported to be either immersion or spin-coating of low concentration PA solutions in methanol or ethanol but the surface coverage by the phosphonic acids remained uncharacterized [24–26]. Tuning the work function of the conductive oxide layer is likely to be very sensitive to the coverage as well as the presence of multilayers or pinholes [19, 20, 29]. Spray-coating methods have been reported to provide self-assembled monolayers of the small molecule pentafluorobenzyl phosphonic acid with good coverage on ITO and indium zinc oxide (IZO) when compared to a 1 h immersion at 75 °C [28]. The coverage was assessed by comparing the corrected F/In atomic ratios measured by X-ray photoelectron spectroscopy and the effect on the work function of ITO and IZO was also evaluated. It was observed that the phosphonic acid molecular dipole contribution saturates at a coverage ca. 65% that of a close-packed monolayer, likely due to depolarization effects [28]. An extensive study [30] of organic SAMs behavior on iron, nickel, chromium, molybdenum, manganese, iron, titanium and their alloy showed that phosphonic acid reacts with all the metals and alloys and remains attached

even after sonication. Spray-coating parameters were comprehensively examined in this article [30].

In a previous work, a concept based on self-assembled monolayers was proposed to obtain patterned nickel lines by electroplating on ITO in order to obtain low-cost conductor grids on heterojunction solar cells [23]. This approach aimed to achieve plating selectivity with ultra-low costs. This application requires modified surfaces with high hydrophobicity and coverage. High dynamic water contact angles with low hysteresis were obtained on ITO surfaces modified by octadecylphosphonic acid (ODPA) and perfluorinated phosphonic acids [23]. In this context, it is necessary to develop large-scale, low-cost protocols that will both reduce processing times and produce covalently bonded monolayers of phosphonic acids on metal oxide surfaces along with uniform coverage. Moreover, it is critical to obtain a very dense monolayer without pinholes otherwise negative effects such as parasitic plating could occur and impact the solar cell efficiency. Spray-coating the PA solution onto ITO is a versatile solution. Raman *et al.* observed that dipping and spraying procedures showed similar organization of the films on metal oxide surfaces [30]. This work investigates the effects of changing the immersion, spraying or rinsing solvent nature in the formation of dense monolayers of a long-chained perfluorinated phosphonic acids using both spraying and immersion processes. ODPA SAMs have been well studied [14, 16, 17, 31–33] and serve as a reference. AFM measurements on ultra-smooth ITO substrates, dynamic contact angle measurements, and attenuated total reflectance Fourier-transform infrared spectroscopy (ATR-FTIR) are used to characterize the SAMs.

2. Materials and methods

Materials: Octadecylphosphonic acid (ODPA) was purchased from Sigma Aldrich (Switzerland). 10,11-Bis(2,2,3,3,4,4,5,5,6,6,7,7,8,8,9,9,9-Heptadecafluorononyl)icosane-1,20-diyldiphosphonic acid (bis-fC19-bis-PA) was purchased from Sikemia (France). The chemical structure of this gemini perfluorinated phosphonic acid is shown in Figure 1. Ethanol (VLSI grade) was purchased from KMG Ultra Pure Chemicals SAS (France). Methoxy-nonafluorobutane (NovecTM 7100, 3M) was purchased from Inventec (Switzerland). All chemicals were used as received.

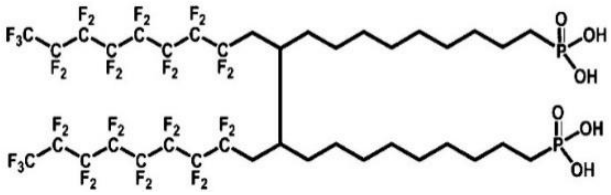

Figure 1: chemical structure of 10,11-Bis(2,2,3,3,4,4,5,5,6,6,7,7,8,8,9,9,9-Heptadecafluorononyl)icosane-1,20-diyldiphosphonic acid (bis-fC19-bis-PA)

Low roughness ITO surfaces (0.2 nm as measured by AFM) were produced by sputtering 20 nm ITO using an Indeotec Octopus II tool on single side polished silicon wafers. The target composition was 90/10 indium oxide/tin oxide by weight. The wafers were supplied by Si-Mat (Germany).

Monolayer deposition: All substrates were cleaned by sonication in isopropanol, followed by sonication in ethanol, for 10 min each, followed by drying in a flow of nitrogen. Oxygen plasma treatment is known to remove carbon contamination from substrates and to increase the amount of surface hydroxylation which in turns increases the amount of phosphonic acid surface coverage [14]. An oxygen plasma was thus performed on all substrates using a PlasmaLab80+ (Oxford Instruments, power: 100 W, pressure: 26.7 Pa, Flow: $8.3.10^{-7}$ m^3/s O_2) and the samples

were either immediately immersed in or sprayed by a solution of 5 mM phosphonic acid in the chosen solvent or solvent mixture. The spray-coating was performed at room temperature using a Nordson spray head with a 781 mini nozzle attached to a Janome dosing system. Stroke was set at 3 with a nozzle air pressure of 3.10^4 Pa and a cartridge pressure of 2.10^4 Pa. Immersion in ethanol was done at 70 °C for 1 h. Immersion in the methoxy-nonafluorobutane and ethanol mixture was done at 50 °C, close to the azeotrope temperature of 52 °C [34]. The excess material was rinsed off with the chosen solvent, dried with nitrogen flow, and the samples were annealed in a low-vacuum oven at 120 °C to promote covalent bonding [35].

Dynamic contact angle measurements: The wettability changes of the surfaces were characterized by measuring the contact angle of water sessile droplets deposited on the sample. Advancing and receding water contact angles were determined using a Drop Shape Analysis System DSA30 provided by Krüss (Hamburg, Germany). Standard deviations were calculated from three measurements and the error bars shown on the graphs correspond to the 95 % confidence intervals.

Atomic force microscopy: AFM analysis of films was performed using a Dimension Icon AFM machine (Brüker) equipped with silicon probes Tap150Al-G from BudgetSensors (resonant frequency 150 kHz, force constant 5 N/m). Measurements were performed with tapping mode in air.

ATR-FTIR measurements: Attenuated total reflectance infrared (ATR-FTIR) spectra were recorded on a Brüker Vertex 70 equipped with a VariGATR single angle reflection accessory (Harricks Scientific) and a liquid-nitrogen cooled MgCdTe detector using 512 scans at a resolution of 4 cm^{-1}. Corresponding background spectra were acquired on ITO-covered silicon

wafers that also underwent the plasma treatment step. The spectra of the corresponding bulk materials (powders) were also acquired using the VariGATR accessory with a background of air.

5. Results and discussion

1. Characterization of ODPA SAM by immersion and spraying

As a reference for the protocol, SAMs of ODPA were prepared with ethanol as both deposition and rinsing solvent. The surfaces appeared clear and transparent after the deposition, rinsing, and annealing steps. The surfaces were characterized by their wettability and AFM measurements before and after SAM deposition.

In order to observe the uniformity of the SAM on the ITO, a roughness that is significantly lower than the thickness of the SAM is required. The roughness of the bare ITO substrate was measured by atomic force microscopy. The AFM image is shown in Figure 2 a. The average roughness on the whole scan was calculated to be 0.2 nm. The advancing and receding water contact angles of bare ITO before oxygen plasma were 89 ± 2 ° and 19 ± 3 °, respectively. After the plasma treatment, the static water contact angle on the surface was below 10 °. The fit of the droplet shape on the instrument does not reliably allow for a more accurate value.

After SAM depositions, the surface was characterized at three different points by its wettability and AFM measurements. The static water contact angle on the surface was found to be 107.7 ± 0.5 ° for immersion and 107 ± 3 ° for spraying. Reported static contact angle for ODPA on ITO is 104 ± 2 ° [35]. Chemical variations in the ITO itself or a different roughness explain the observed difference. The advancing and receding water contact angles were 116.5 ± 0.6 ° and 95

± 1 ° for immersion and 113.1 ± 0.2° and 95 ± 3 ° for spraying. These results are consistent with a highly homogenous, very dense SAM and are similar to the results obtained for ODPA SAMs on alumina films deposited on polished silicon surfaces [36–38]. The uniformity of the ODPA SAM was determined by AFM measurement. Typical images are shown in Figure 2 b and c. For SAM prepared by immersion, the average roughness measured on the whole AFM scan was calculated to be 0.2 nm indicating a high conformality of the ODPA SAM. In the case of spraying the ODPA to prepare the SAM, a few aggregates of approximatively 2.5 nm average height are observed on all images. Aggregate average density (on three images) is ≤ 50 particles §per μm^2. The surface of the SAM below these aggregates is uniform and homogenous with low roughness. The extended length of the ODPA molecule on the surface being calculated at 2.9 nm, these aggregates correspond to one layer of molecules. These low height aggregates have only been observed after this specific spraying and rinsing process. Harsher rinsing procedures, *e.g.* ultrasons, could remove them if necessary.

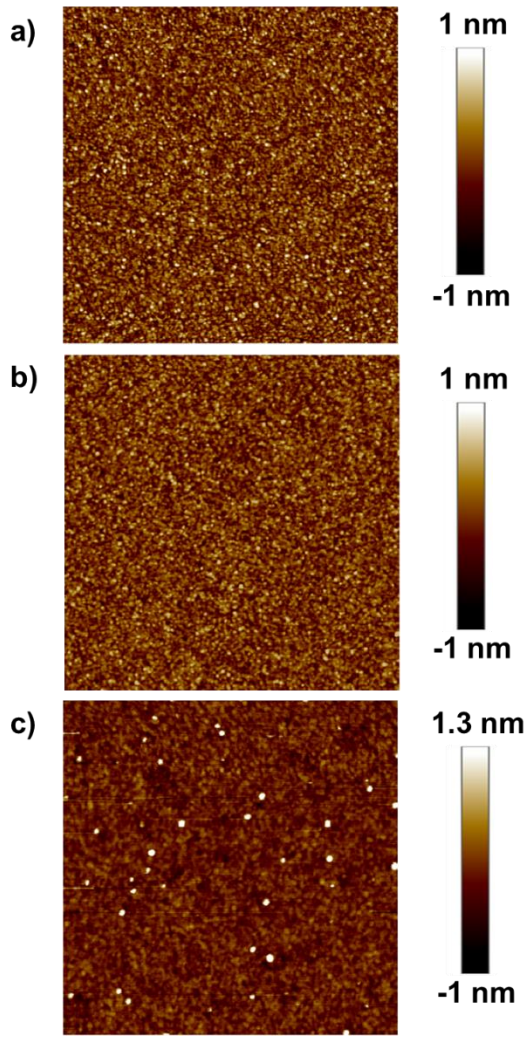

Figure 2. AFM image (scan area: 1 µm x 1 µm) a) of the bare ITO, b) of an ODPA SAM prepared by immersion in ethanol for 1 h at 70 °C, and c) of an ODPA SAM prepared by spraying in ethanol and rinsing in the same solvent. The height scale bar is next to each the image.

Insights in the formation of an ODPA SAM on the ITO is gained by attenuated total reflectance Fourier-Transform InfraRed (ATR-FTIR) characterization. Spectra of the SAMs on ITO substrates were recorded and compared to the spectrum of bulk ODPA powder (Figure 3).

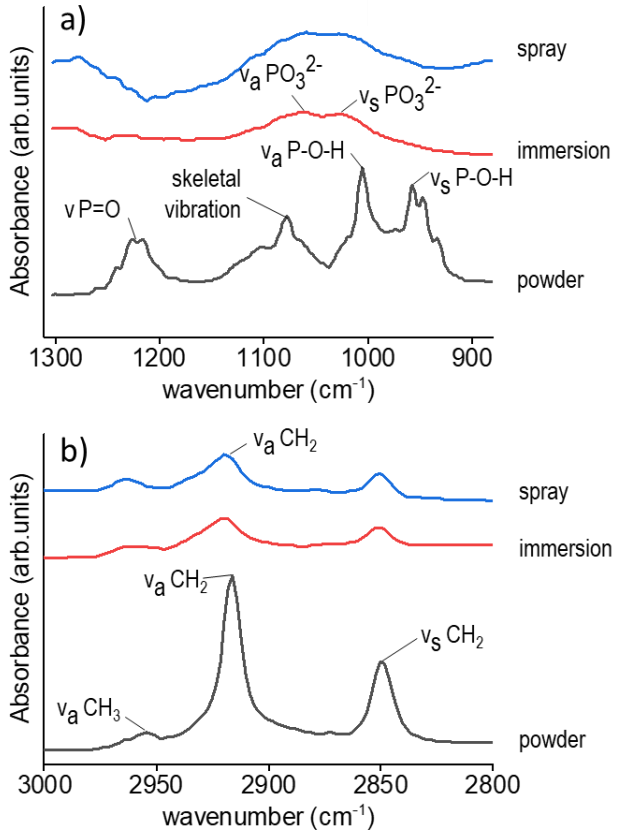

Figure 3: a) comparisons of the ODPA FTIR spectrum (bottom) and the spectra for ODPA-modified ITO surfaces (top spectra) in the ν_{P-O} region, with assignments as described in references [32, 39]. b) same spectral comparisons for the ν_{C-H} region.

On the ODPA powder spectrum, peaks for the νP=O, ν_aP-O(-H) and ν_sP-O(-H) vibrations are observed at 1230, 1005 and 956 cm^{-1}, respectively. The peaks are clearly different for the surface-bound versus the bulk material. The spectra of the ODPA SAMs on ITO suggest mainly a tridentate binding of the phosphonic acid to the ITO since no νP=O can be observed while broad peaks are observed in the ν PO_3^{2-} region (ν_a PO_3^{2-} is situated around 1066 cm^{-1} and ν_s PO_3^{2-} 1030 cm^{-1}) [32, 33, 39].

In the ν_{C-H} region on the powder spectrum, peaks for ν_a CH_3, ν_a CH_2 and ν_s CH_2 vibrations are observed at 2954, 2916 and 2850 cm^{-1} respectively. On hydroxylated surfaces with well-

organized monolayers, asymmetric and symmetric bands are expected at 2918 and 2849 cm^{-1}, respectively [40]. These exact peaks are observed on the ODPA-modified ITO, either by spraying or immersion coating, indicating a well-ordered SAM on the surface.

2. Preparation of perfluorinated PA SAMs by immersion

Perfluorinated PA SAMs have been previously studied on various surfaces, such as Mica [41], Mg [18], ZnO [22], [42] and ITO [23]. On ZnO, these films were shown to remain strongly bonded on the surfaces after sonication and after two years [42].

SAMs of bis-f-C19-bis-PA were prepared by immersion in either ethanol or a mixture of ethanol and methoxy-nonafluorobutane (MNFB). MNFB was chosen for its affinity with the perfluorinated chains of the phosphonic acid molecules, while ethanol is a known solvent for phosphonic acids dissolution. It was observed that the perfluorinated PA did not dissolve properly at 5 mmol/L in pure MNFB due to the amphiphilicity of the molecule. A small addition of ethanol as a co-solvent permitted its dissolution. The rinsing solvent was also changed from ethanol to MNFB.

The SAMs were then characterized by water contact angle measurements. The static water contact angles are given in Table 1. The rinsing or immersion solvent used in the SAM preparation did not create a significant difference in the measured static water contact angle. The static water contact angle for bis-f-C19-bis-PA has not been reported previously. The reported static water contact angle for 3,3,4,4,5,5,6,6,7,7,8,8,8-tridecafluorooctylphosphonic acid (FOPA) was reported to be 108 ± 2 ° by Sharma *et al.* [35] while Trabelsi *et al.* obtained a static water contact angle of 91 ° on a perfluorinated C19 chain (f-C19-PA) on mica [41]. Bis-f-C19-bis-PA

SAMs produce significantly more hydrophobic surfaces than FOPA and f-C19-PA which can be explained by a better homogeneity, longer perfluorinated chains, differences in phosphonic acid anchoring on ITO and mica, and a better arrangement of the chains in the SAM due to the gemini-surfactant-like structure of the molecule.

Table 1. Static water contact angles for a bis-f-C19-bis-PA SAM prepared with various immersion and rinsing solvents.

Immersion solvent	Rinsing solvent	Static water contact angle
Ethanol	Ethanol	121.6 ± 0.8 °
Ethanol	MNFB [a)]	117 ± 1 °
MNFB 93% v/v and ethanol 7% v/v	MNFB	119 ± 1 °

[a)] MNFB stands for methoxy-nonafluorobutane

The dynamic water contact angles measured on these three SAMs are shown in Figure 3. No significant difference was observed between the samples prepared in different experimental conditions. The hysteresis between the advancing and receding water contact angles is comparatively low (between 14 ° and 17 °) when the ODPA SAMs showed a hysteresis of 21 °. The stability of the monolayers over time was also investigated as shown in Figure 3. The dynamic contact angles of the deposited layers did not change over 15 months, indicating an excellent stability of the SAMs. The samples were kept at room temperature in a laboratory environment with no specific precautions.

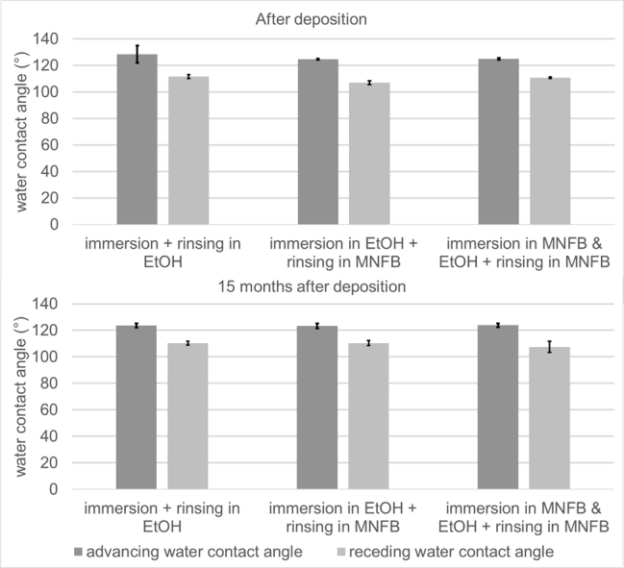

Figure 4: advancing and receding water contact angles measured on SAMs of bis-f-C19-bis-PA prepared with different immersion and rinsing solvents. Top: the dynamic water contact angles were measured immediately after deposition; bottom: the measurements were taken on the samples 15 months after the deposition of the SAMs.

The effect of rinsing and immersion solvents was further investigated by AFM measurements as shown in Figure 5. On the AFM images corresponding to a SAM prepared and rinsed with ethanol as a solvent, many particles can be seen on the surface with spots with up to 15 nm-high aggregates. On Figure 5 a 180 particles per μm^2 were measured on the image with an average height of 4.5 nm. This figure is typical of the AFM images taken on this surface. Since the length of a fully extended molecule of bis-fC19-bis-PA is calculated to be 3.2 nm, these particles are thought to be micellar aggregates of the molecule bis-fC19-bis-PA which form in ethanol. In Figure 5 b larger areas of height measured between 4.5 and 5 nm are observed on the bottom of the image. Given the high contact angle values and the low hysteresis between the advancing and receding contact angles measured on this surface, the surface is thought to be covered in a dense monolayer of bis-fC19-bis-PA with bilayers across the surface as well some multilayered aggregates in places.

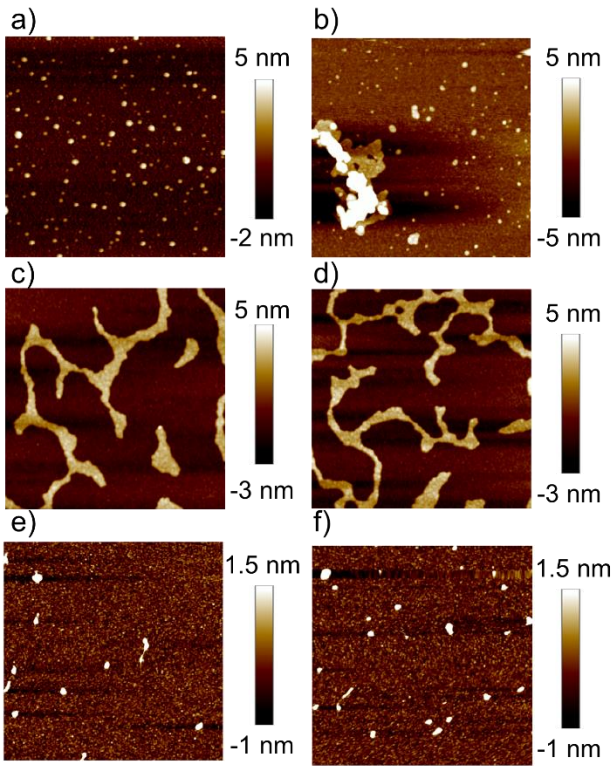

Figure 5: AFM images (a; c-f with scan area: 1 µm x 1 µm; b with scan area: 850nm x 850nm) of bis-fC19-bis-PA SAMs prepared by immersion. Images a) and b) correspond to a SAM with ethanol as both immersion and rinsing solvents, c) and d) correspond to a SAM with ethanol as immersion solvent and MNFB as rinsing solvent; while e) and f) correspond to a SAM with 93% MNFB and 7% ethanol as immersion solvent, and MNFB as rinsing solvent. The height scale bar is inserted in the top right of each image.

Figures 5 c and d correspond to a SAM prepared with ethanol as a solvent but rinsed with MNFB. Surprisingly, typical “spinodal dewetting” patterns are observed on this surface [43]. Spinodal dewetting, in analogy to spinodal decomposition of incompatible liquids, corresponds to the spontaneous dewetting of extremely thin liquid films due to the amplification of thermal fluctuations. The height of these pattern is very homogenous with an average at 4.7 nm. In Figure 5 c the higher patterns occupy 17 % of the total image area and on Figure 5 d the patterns correspond to 20 % of the total area. This height is similar to the height of the small aggregates observed in Figures 5a and 5b. A schematic of these multilayers is shown in Figure 6.

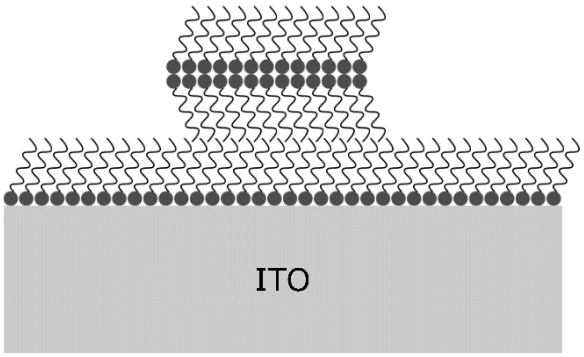

Figure 6: schematics of the interpreted molecular structure of the dewetting patterns observed on the AFM images taken for bis-fC19-bis-PA SAMs on ITO.

Finally, Figures 5 e) and f) show the surface of a sample prepared with MNBF as both the immersion and rinsing solvent. A few particles, from 12 to 30 per μm^2, of height around 5 nm are still observed on the surface, but this is the flattest SAM obtained on ITO using bis-fC19-bis-PA. This observation correlates well with the low hysteresis observed between advancing and receding contact angles (see Figure 4).

The dewetting phenomenon occurs on a surface already covered by a self-assembled monolayer of bis-f-C19-bis-PA when immersed in ethanol, dried, and rinsed off with a fluorinated solvent. MNBF is extremely volatile, has a low surface tension of 13.6 mN/m, and is a poorer solvent to bis-f-C19-bis-PA than ethanol. When both immersion and rinsing steps are carried in ethanol, aggregates occur. The excess molecules covering the surface after immersion are picked up by the rinsing solvent. In ethanol, molecules go at its surface due to their surfactant properties and form micellar-like aggregates when drying. When carrying out the whole process in MNBF, less aggregates are created, and a smoother surface is observed. This indicates that the organizations of the molecules in the ethanol-immersed and MNBF mixture-immersed SAMs differ. When rinsing off the ethanol immersed SAM with MNBF, the difference in self-organization could

create a dewetting pattern. Moreover, drying dynamics with MNBF create a faster drying step with less surface-tension driven interactions [44]. The influence of these parameters on the pattern observed are yet unknown but are of interest for a future study.

The perfluorinated PA monolayers were then further characterized by ATR-FTIR. Two regions of the IR spectrum show characteristic bands for perfluoroalkyl phosphonic acids such as bis-fC19-bis-PA. One is the C-H stretching region ranging from 2800 to 3000 cm^{-1} and the other is the C-F stretching region ranging from 900 to 1400 cm^{-1}. The second interval intersects with the ν_{P-O} region (900 to 1300 cm^{-1}). Spectra for bis-f-C19-bisPA powder and SAMs prepared with the various conditions described previously are compared in Figure 7.

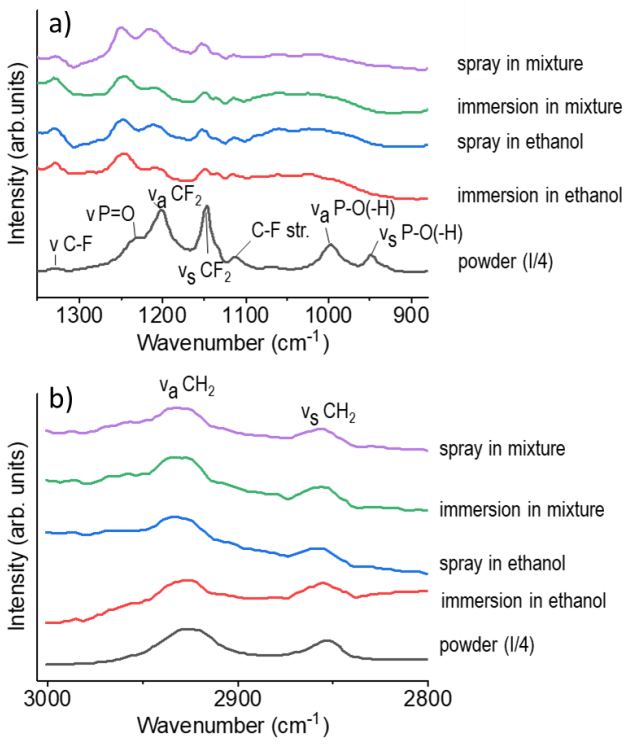

Figure 7: a) comparisons of the bulk bis-f-C19-bisPA FTIR absorbance spectrum (bottom) and the absorbance spectra for bis-f-C19-bisPA -modified ITO surfaces (top spectra) in the ν_{P-O} and ν_{C-F} region, with assignments as described in references [26] and [35]. The intensity of the

powder spectrum was divided arbitrarily by 4 for the sake of graphical clarity. Figure b) same spectral comparisons for the ν_{C-H} region.

On the bis-fC19-bisPA powder spectrum, peaks for the νP=O, ν_aP-O(-H) and ν_sP-O(-H) vibrations are observed at 1230, 997 and 949 cm^{-1} respectively, only slightly shifted when compared to the ODPA powder spectrum. On all the surface-bound bis-fC19-bisPA spectra, peaks at 1235 cm^{-1} attributed to νP=O and slightly shifted compared to the powder spectrum, are observed as well as broad peaks, less defined, at 1060 and 1025 cm^{-1}. The latter peaks are in the regions of either the ν PO_3^{2-} or the νPO_2^- vibrations. The presence of a νP=O peak indicates thus mostly bidentate bonds [32, 39] potentially mixed with some tridentate bonds. This is attributed to a different organization of perfluoralkyl versus alkyl chains in the SAMs. The strong IR bands at 1201 and 1147 cm^{-1} have been assigned to both the asymmetric and symmetric stretching vibrations of the CF_2 group [39, 40]. A weaker band at 1113 cm^{-1} is attributed to the axial CF_2 stretching while the band at 1326 cm^{-1} is attached to the stretching vibrations of the CF_3 end group [39]. Peak intensities of the νP=O, ν_a CF_2, and ν_s CF_2 also vary between the powder and the bound materials. These changes are interpreted as a result of changes in the organization of the perfluoroalkyl chains when bound to the ITO surface. SAMs containing perfluoroalkyl chains have been described as possessing a helical structure with less ordered chains [40].

In the ν_{C-H} region on the powder spectrum, peaks for ν_a CH_2 and ν_s CH_2 vibrations are observed at 2927 and 2852 cm^{-1}, respectively. The shift when compared to well-organized alkyl monolayers, where asymmetric and symmetric bands are expected at 2918 and 2849 cm^{-1} (see Figure 3) has been observed previously [40] indicating some disorganization in the layers. The spectra of all SAMs, whether prepared by spraying or immersion in various solvents, show

similar peaks and peak intensity, indicating similar structural properties for all prepared monolayers.

In this study, two main approaches have been used for the deposition of phosphonic acid SAMs on ITO surfaces: immersion and spray coating. The long-term objective of this study being the development of coating processes for the photovoltaic industry, a critical point is the to cover full wafers (150 mm) with a high throughput and cost-effective process. With the parameters used in this study, the immersion process had a throughput of 1 wafer per hour and required a volume of solution of at least 250 mL. For the spray coating process, a full wafer was processed in 200 s, corresponding to a throughput of 17 wafers per hour and a volume of solution of 1.5 mL per wafer was required. On a production standpoint, immersion could be upscaled by processing batches of wafers, leading to a throughput of 25 wafers per hour for standard batch sizes. However, a large amount of solution would be needed for example to fill a 30 L tank. For the spray coating process, the throughput could be augmented even further by either increasing the deposition speed or by using specific spray shapes (fan type) allowing the single pass deposition of the phosphonic acid.

6. Conclusion

It is demonstrated that gemini perfluorinated phosphonic acid provide high coverage and hydrophobicity on flat indium tin oxide surfaces. Both spray-coating and immersion methods provided high coverage of SAMs on ITO. However, aggregates and multilayers were observed depending on the solvents used for the deposition and rinsing steps. Multilayers were observed when the rinsing solvent has a low solvation of the long perfluorinated chains, but the influence of the immersion solvent seemed less critical to obtain high coverage of SAMs. The coverage of

the SAM was characterized by atomic force microscopy while the hydrophobicity of the layers was measured by means of static and dynamic water contact angles on the surface. The chemical binding of the phosphonic acids was investigated by ATR-FTIR and observed peaks were assigned to bidentate bonds with the ITO. The quality of the SAMs obtained by spray-coating give the potential for these SAMs to be used for low-cost, scalable, rapid manufacturing, and patterning of conductive grids of solar cells as described in previous work [23].

7. Authors' contributions

The manuscript was written through contributions of all authors. GALA designed the experimental work, proceeded to immersion experiments, recorded FTIR spectra, measured contact angles, analyzed the raw AFM data, and wrote the article and all revisions to the article. NB and JG developed the spray-coated samples and contributed to analysis and characterization. SU acquired all AFM data. AL and AF contributed to experiments design, tests, and analysis. GALA, AL and AF were involved in fund acquisition and project administration.

8. Acknowledgements

This work was funded by the Swiss National Science Foundation (SNSF) in the AMELIZ project. The authors are thankful to Dr. Gabriel Christmann for the deposition of ITO onto single side polished silicon wafers and to Dr. Nicholas Hendricks for corrections to the manuscript.

9. Bibliography

[1] G. M. Whitesides, J. K. Kriebel, and J. C. Love, "Molecular engineering of surfaces using self-assembled monolayers," *Sci. Prog.*, vol. 88, no. 1, pp. 17–48, Feb. 2005.

[2] A. G. Koutsioubas, N. Spiliopoulos, D. L. Anastassopoulos, A. A. Vradis, and G. D. Priftis, “Formation of alkane-phosphonic acid self-assembled monolayers on alumina: An in situ SPR study,” *Surf. Interface Anal.*, vol. 41, no. 11, pp. 897–903, 2009.

[3] S. P. Pujari, L. Scheres, A. T. M. Marcelis, and H. Zuilhof, “Covalent Surface Modification of Oxide Surfaces,” *Angew. Chem. Int. Ed. Engl.*, vol. 53, pp. 6322–6356, 2014.

[4] J. C. Love, L. A. Estroff, J. K. Kriebel, R. G. Nuzzo, and G. M. Whitesides, “Self-assembled monolayers of thiolates on metals as a form of nanotechnology,” *Chem. Rev.*, vol. 105, no. 4, pp. 1103–1169, 2005.

[5] Y. Xue, X. Li, H. Li, and W. Zhang, “Quantifying thiol-gold interactions towards the efficient strength control,” *Nat. Commun.*, vol. 5, 2014.

[6] D. S. Karpovich and G. J. Blanchard, “Direct Measurement of the Adsorption Kinetics of Alkanethiolate Self-Assembled Monolayers on a Microcrystalline Gold Surface,” *Langmuir*, vol. 10, no. 9, pp. 3315–3322, 1994.

[7] A. Ulman, “Formation and Structure of Self-Assembled Monolayers.,” *Chem. Rev.*, vol. 96, no. 4, pp. 1533–1554, Jun. 1996.

[8] N. L. Jeon, R. G. Nuzzo, Y. Xia, M. Mrksich, and G. M. Whitesides, “Patterned self-assembled monolayers formed by microcontact printing direct selective metalization by chemical vapor deposition on planar and nonplanar substrates,” *Langmuir*, vol. 11, no. 8, pp. 3024–3026, Aug. 1995.

[9] S. R. Wasserman, Y. T. Tao, and G. M. Whitesides, "Structure and Reactivity of Alkylsiloxane Monolayers Formed by Reaction of Alkyltrichlorosilanes on Silicon Substrates," *Langmuir*, vol. 5, no. 4, pp. 1074–1087, 1989.

[10] D. Janssen, R. De Palma, S. Verlaak, P. Heremans, and W. Dehaen, "Static solvent contact angle measurements, surface free energy and wettability determination of various self-assembled monolayers on silicon dioxide," *Thin Solid Films*, vol. 515, no. 4, pp. 1433–1438, Dec. 2006.

[11] S. Tosatti, R. Michel, M. Textor, and N. D. Spencer, "Self-assembled monolayers of dodecyl and hydroxy-dodecyl phosphates on both smooth and rough titanium and titanium oxide surfaces," *Langmuir*, vol. 18, no. 9, pp. 3537–3548, 2002.

[12] D. M. Spori, N. V. Venkataraman, S. G. P. Tosatti, F. Durmaz, N. D. Spencer, and S. Zürcher, "Influence of alkyl chain length on phosphate self-assembled monolayers," *Langmuir*, vol. 23, no. 15, pp. 8053–8060, 2007.

[13] J. T. Woodward, A. Ulman, and D. K. Schwartz, "Self-assembled monolayer growth of octadecylphosphonic acid on mica," *Langmuir*, vol. 12, no. 15, pp. 3626–3629, 1996.

[14] S. A. Paniagua *et al.*, "Phosphonic Acids for Interfacial Engineering of Transparent Conductive Oxides," *Chem. Rev.*, vol. 116, no. 12, pp. 7117–7158, 2016.

[15] E. Kristan Mioč and H. Otmačić Ćurković, "Protective films of stearic and octadecylphosphonic acid formed by spray coating," *J. Electrochem. Sci. Eng.*, vol. 10, no. 2, p. 161, 2020.

[16] R. Quiñones, A. Raman, and E. S. Gawalt, "Functionalization of nickel oxide using alkylphosphonic acid self-assembled monolayers," *Thin Solid Films*, vol. 516, no. 23, pp. 8774–8781, 2008.

[17] T. L. Breen, P. M. Fryer, R. W. Nunes, and M. E. Rothwell, "Patterning indium tin oxide and indium zinc oxide using microcontact printing and wet etching," *Langmuir*, vol. 18, no. 1, pp. 194–197, 2002.

[18] T. Ishizaki, K. Teshima, Y. Masuda, and M. Sakamoto, "Liquid phase formation of alkyl- and perfluoro-phosphonic acid derived monolayers on magnesium alloy AZ31 and their chemical properties," *J. Colloid Interface Sci.*, vol. 360, no. 1, pp. 280–288, 2011.

[19] I. Lange *et al.*, "Tuning the work function of polar zinc oxide surfaces using modified phosphonic acid self-assembled monolayers," *Adv. Funct. Mater.*, vol. 24, no. 44, pp. 7014–7024, 2014.

[20] G. Ramanath, M. Kwan, P. K. Chow, Y. C. Quintero, P. H. Mutin, and R. Ramprasad, "Tuning of noble metal work function with organophosphonate nanolayers," *Appl. Phys. Lett.*, vol. 105, no. 8, 2014.

[21] S. A. Paniagua, E. L. Li, and S. R. Marder, "Adsorption studies of a phosphonic acid on ITO: Film coverage, purity, and induced electronic structure changes," *Phys. Chem. Chem. Phys.*, vol. 16, no. 7, pp. 2874–2881, 2014.

[22] J. L. Braid, U. Koldemir, A. Sellinger, R. T. Collins, T. E. Furtak, and D. C. Olson, "Conjugated Phosphonic Acid Modified Zinc Oxide Electron Transport Layers for Improved Performance in Organic Solar Cells," *ACS Appl. Mater. Interfaces*, vol. 6, p.

19229−19234, 2014.

[23] G. A. L. Andreatta, A. Lachowicz, N. Blondiaux, C. Allebé, and A. Faes, “Patterning solar cell metal grids on transparent conductive oxides using self-assembled phosphonic acid monolayers,” *Thin Solid Films*, vol. 691, 2019.

[24] A. Magomedov *et al.*, “Self-Assembled Hole Transporting Monolayer for Highly Efficient Perovskite Solar Cells,” *Adv. Energy Mater.*, vol. 8, no. 32, pp. 1–24, 2018.

[25] A. Al-Ashouri *et al.*, “Conformal monolayer contacts with lossless interfaces for perovskite single junction and monolithic tandem solar cells,” *Energy Environ. Sci.*, vol. 12, no. 11, pp. 3356–3369, 2019.

[26] R. B. M. Hill *et al.*, “Phosphonic Acid Modification of the Electron Selective Contact: Interfacial Effects in Perovskite Solar Cells,” *ACS Appl. Energy Mater.*, vol. 2, no. 4, pp. 2402–2408, 2019.

[27] A. Al-Ashouri *et al.*, “Monolithic perovskite/silicon tandem solar cell with 29% efficiency by enhanced hole extraction,” *Science (80-.).*, vol. 370, no. December, pp. 1300–1309, 2020.

[28] A. Bulusu *et al.*, “Efficient modification of metal oxide surfaces with phosphonic acids by spray coating,” *Langmuir*, vol. 29, no. 12, pp. 3935–3942, 2013.

[29] S. Y. Abate, D. C. Huang, and Y. T. Tao, “Surface modification of TiO2 layer with phosphonic acid monolayer in perovskite solar cells: Effect of chain length and terminal functional group,” *Org. Electron.*, vol. 78, p. 105583, 2020.

[30] A. Raman, R. Quiñones, L. Barriger, R. Eastman, A. Parsi, and E. S. Gawalt, "Understanding Organic Film Behavior on Alloy and Metal Oxides," *Langmuir*, vol. 582, no. 41, pp. 1747–1754, 2010.

[31] E. S. Gawalt, M. J. Avaltroni, N. Koch, and J. Schwartz, "Self-assembly and bonding of alkanephosphonic acids on the native oxide surface of titanium," *Langmuir*, vol. 17, no. 19, pp. 5736–5738, 2001.

[32] S. A. Paniagua *et al.*, "Phosphonic acid modification of indium-tin oxide electrodes: Combined XPS/UPS/ contact angle studies," *J. Phys. Chem. C*, vol. 112, no. 21, pp. 7809–7817, 2008.

[33] M. Giza, P. Thissen, and G. Grundmeier, "Adsorption kinetics of organophosphonic acids on plasma-modified oxide-covered aluminum surfaces," *Langmuir*, vol. 24, no. 16, pp. 8688–8694, 2008.

[34] C. Hansen and J. Durkee, "Use of Hansen Solubility Parameters to Identify Cleaning Applications for 'Designer' Solvents," in *Hansen Solubility Parameters: a user's hanbook*, no. June 2007, 2007, pp. 203–229.

[35] A. Sharma, B. Kippelen, P. J. Hotchkiss, and S. R. Marder, "Stabilization of the work function of indium tin oxide using organic surface modifiers in organic light-emitting diodes," *Appl. Phys. Lett.*, vol. 93, no. 16, pp. 111–114, 2008.

[36] H. Y. Nie, N. S. McIntyre, W. M. Lau, and J. M. Feng, "Optical properties of an octadecylphosphonic acid self-assembled monolayer on a silicon wafer," *Thin Solid Films*, vol. 517, no. 2, pp. 814–818, 2008.

[37] I. L. Liakos, R. C. Newman, E. McAlpine, and M. R. Alexander, “Study of the resistance of SAMs on Aluminium to Acidic and Basic Solutions using Dynamic Contact Angle Measurement,” *Langmuir*, vol. 23. pp. 995–999, 2007.

[38] H.-Y. Y. Nie, M. J. Walzak, and N. S. McIntyre, “Delivering Octadecylphosphonic Acid Self-Assembled Monolayers on a Si Wafer and Other Oxide Surfaces,” *J. Phys. Chem. B*, vol. 110, no. 42, pp. 21101–21108, 2006.

[39] G. Socrates, *Infrared and Raman characteristic group frequencies. Tables and charts*. 2001.

[40] C. K. Luscombe, H. Li, W. T. S. Huck, and A. B. Holmes, “Fluorinated Silane Self-Assembled Monolayers as Resists for Patterning Indium Tin Oxide,” *Langmuir*, vol. 19, no. 24, pp. 5273–5278, 2003.

[41] S. Trabelsi, S. Zhang, Z. Zhang, T. R. Lee, and D. K. Schwartz, “Semi-fluorinated phosphonic acids form stable nanoscale clusters in Langmuir-Blodgett and self-assembled monolayers,” *Soft Matter*, vol. 5, no. 4, pp. 750–758, 2009.

[42] R. Quiñones *et al.*, “Study of Perfluorophosphonic Acid Surface Modifications on Zinc Oxide Nanoparticles,” *Materials (Basel).*, vol. 10, pp. 1363–1379, 2017.

[43] R. Seemann, S. Herminghaus, and K. Jacobs, “Gaining control of pattern formation of dewetting liquid films,” *J. Phys. Condens. Matter*, vol. 13, no. 21, pp. 4925–4938, 2001.

[44] S. L. Manzello and J. C. Yang, “An experimental study of high Weber number impact of methoxy-nonafluorobutane C4F9OCH3 (HFE-7100) and n-heptane droplets on a heated

solid surface," *Interrnational J. Heat Mass Transf.*, vol. 45, pp. 3961–3971, 2002.